ARTICLES

Journal of Semiconductors
(2020) 41, 052203
doi: 10.1088/1674-4926/41/5/052203

Mo^{5+} doping induced interface polarization for improving performance of planar perovskite solar cells

Yurong Jiang†, Yue Yang, Yiting Liu, Shan Yan, Yanxing Feng, and Congxin Xia†

School of Physics, Henan Key Laboratory of Photovoltaic Materials, Henan Normal University, Xinxiang 453007, China

Abstract: In this paper, we investigate how interface-induced polarization affects the photovoltaic performance of hybrid perovskite solar cell (PSC) devices. The polarization of the hole transport layer (HTL) is regulated through incorporating metallic-like MoO_x into PEDOT:PSS. The common MoO_3 doped into PEDOT:PSS is used as a reference, and the device that used PEDOT:PSS-MoO_x as the HTL shows an enhanced J_{sc} and FF compared to the reference device. The open-circuit photovoltage decay and impedance spectroscopy measurements indicate that trap-assisted recombination is effectively suppressed at the interface between the hybrid perovskite and the PEDOT:PSS-MoO_x HTL, while severe trap assisted recombination takes place at the perovskite/PEDOT:PSS and perovskite/PEDOT:PSS-MoO_3 interface. We attribute these experimental findings to the fact that the incorporation of metallic-like Mo^{5+} into PEDOT:PSS enhances the conductivity of HTL and the interface polarization between PEDTOT:PSS layer and perovskite, which helps to induce an interface polarization electric field to facilitate separation of charges and screen the recombination between the traps and free charges.

Key words: conductivity; hole-transporting layer; dielectric constant; polarization

Citation: Y R Jiang, Y Yang, Y T Liu, S Yan, Y X Feng, and C X Xia, Mo^{5+} doping induced interface polarization for improving performance of planar perovskite solar cells[J]. *J. Semicond.*, 2020, 41(5), 052203. http://doi.org/10.1088/1674-4926/41/5/052203

1. Introduction

Perovskite solar cells are considered to be promising photovoltaic devices thanks to their excellent properties, such as low cost[1], high efficiency[2], and solution processability[3, 4]. To further boost the photo-conversion efficiency (PCE), both the hole transport layer (HTL)1)[5, 6] and electron transport layer (ETL)[7–10] are employed in perovskite solar cells (PSC). This interfacial engineering could effectively and sufficiently extract the photo-generated holes and electrons from the perovskite active layer and transport them to the corresponding electrodes; thus, PSCs have reached certified efficiencies of over 22.7%[11]. To further improve the PCEs of PSCs, the interfacial engineering of the HTL for hole extraction, transport, and collection from the perovskite layer is an ongoing focus[12–16]. One example is a device structure of ITO/PEDOT:PSS (poly(3,4ethylenedioxythiophene) polystyrene sulfonate)/perovskite/PC61BM/Ag, where PEDOT:PSS are used as the HTL[17, 18]. However, due to electrical inhomogeneity that results from the electrical conductivity gradient from the near surface region to the bulk, and the large microstructure in PEDOT:PSS film morphology (order-of-magnitude variations), the ability of charge transfer within the PEDOT:PSS layer is weakened[19]. Therefore, the electrical conductivity of the PEDOT:PSS layer is lower than that of common metal cathodes[1]. In the PSCs, the poor conductivity of HTL leads to an unbalanced charge carrier transport and the accumulation of charge carriers[20–23]. In addition, the poor electrical conductivity of the HTL layer causes a large series resistance, which results in energy loss during the process of charge carrier transport within the PEDOT:PSS HTL and diminishes the photocurrent and the PCEs of PSCs[5, 24]. An effective hole transport layer with a good conductivity may further improve the photocurrent and FF of PSCs. However, the relative research on optimizing the conductivity of PEDOT:PSS HTL has rarely been reported[25, 26].

In our previous work[27], it was found that doping MoO_x in PEDOT:PSS could improve the coverage of the perovskite layer and then obtain the better PCEs. However, the effect of doped MoO_x on electrical conductivity and interface polarization of HTL hs not received much attention. In this work, we further found that a trace amount of MoO_x not only led to a dramatical enhancement of electrical conductivity of the PEDOT:PSS HTL, which provided an efficient pathway for hole extraction, transport, and collection from the perovskite active layer to the ITO anode, but also resulted in an enhanced interface induced polarization between PEDTOT:PSS layer and perovskite. The short-circuit current density (J_{sc}) was significantly enhanced (from 17.75 to 19.64 mA/cm^2), the open-circuit voltage (V_{oc}) had a slight increase (from 0.96 to 1.01 V), and the FF was significantly enhanced from 0.65 to 0.76, which all resulted in a dramatically enhanced PCE of 15.01%. Compared with the reference PSCs, the PCE had an ~36% enhancement. Moreover, the PSCs with the PEDOT:PSS-MoO_x HTL possessed high device reproducibility. We attributed these experimental results to the fact that the Mo^{5+} could enhance the interfacial polarization of PEDOT:PSS, which possesses a higher conductivity and a larger dielectric constant. The higher interfacial polarization between the perovskite and HTL could facilitate the separating of photo generated holes and electrons and thus suppress the recombination between the traps and free charges. Therefore, the obtained

Correspondence to: Y R Jiang, jiangyurong@whut.edu.cn; C X Xia, xiacongxin@htu.edu.cn

Received 1 MARCH 2020; Revised 23 MARCH 2020.

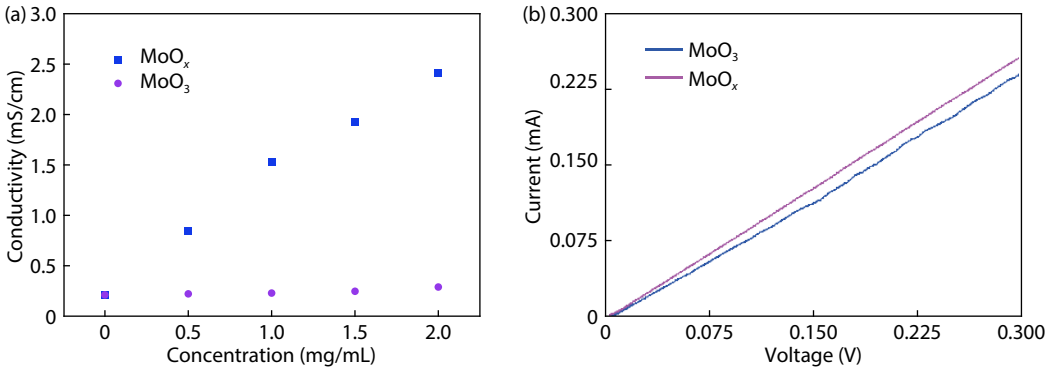

Fig. 1. (Color online) (a) The in-plane conductivity of HTL films with 0–2 mg/mL MoO_x or MoO_3 incorporated into PEDOT:PSS. (b) *I–V* curves test for Ag/MoO_3/ITO and Ag/MoO_x/ITO.

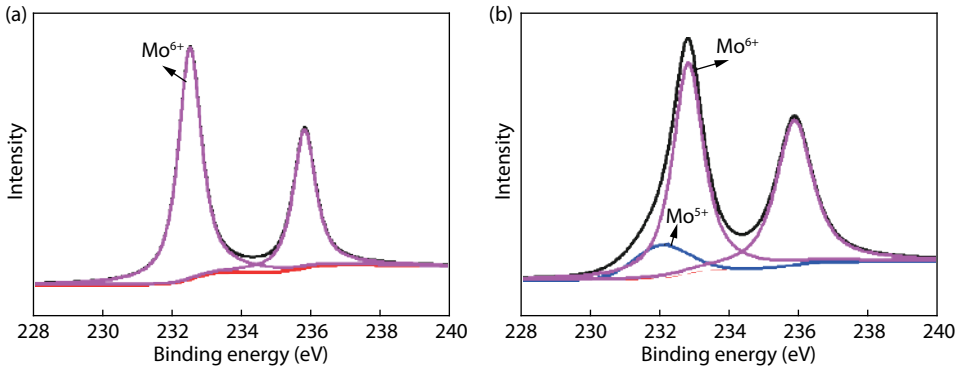

Fig. 2. (Color online) XPS profiles of (a) MoO_3 and (b) MoO_x.

results give an effective strategy to build efficient hole transporting materials for improving the photovoltaic performance of PSCs.

2. Experimental section

2.1. MoO_x synthesis

First, 0.2 g of molybdenum powder (purchased from Aladdin) was dispersed in 20 mL ethanol and oscillated for 30 min in an ultra-sound bath. Then 0.7 mL hydrogen peroxide (H_2O_2) (30%) solution was added into the mixture. Ethanol was used to control the reaction rate between molybdenum powders and H_2O_2. After 20 h of reaction, the mix solution turned from gray to blue. Finally, the mix solution was vaporized in a dry box.

2.2. Conductivity enhancement using MoO_x

The detailed processing and characterization of planar perovskite devices have been reported in our previous work[27]. The MoO_3 was acquired from Sigma-Aldrich (99.999%). It is well-known that the commercially available MoO_3 nanoparticles are slightly soluble in water[28]. However, we found it easy to add into the PEDOT:PSS solution. The ability of MoO_3 as a carrier-selective material depends on its specific electronic properties[29]. Since its energy bandgap (E_{gap}) lies within the O_{2p}- and metal d-bands, its conductivity and work function value depend on the occupancy of the d-states. The N-type MoO_x semiconductivity depends on the intrinsic oxygen vacancies in the atomic structure of MoO_{3-x}, that is, the fully stoichiometric configuration of MoO_3 is insulators and MoO_2 is metallic-like conductors[30].

The conductivity of HTL films with 0–2 mg/mL MoO_x doped in PEDOT:PSS was tested using a four-point probe (Fig. 1(a)). Deposition and measurement of the films were performed in atmosphere under conditions. A significant increase in conductivity from 2.1×10^{-4} to 2.4×10^{-3} S/cm was observed. In addition, the conductivity of PEDOT:PSS-MoO_x was obviously better than that of the PEDOT:PSS-MoO_3. This indicates that the enhanced conductivity of HTL films is linear to MoO_x concentration. It is well-known that the number of O vacancies in MoO_x is larger than that of fully stoichiometric configuration of MoO_3. Therefore, the fact of enhancing conductivity of PEDOT:PSS-MoO_x is consistent to the previous report that the O vacancies determine the conductivity of MoO_x[30]. To further prove the improvement of conductivity originating from the incorporation of MoO_x, the *I–V* curves of Ag/PEDOT:OSS-MoO_3/ITO and Ag/PEDOT:OSS-MoO_x/ITO were performed as shown in Fig. 1(b). The slope of Ag/MoO_x/ITO is higher than that of Ag/MoO_x/ITO, which indicates that the conductivity of PEDOT:OSS-MoO_x is higher than that of PEDOT:OSS-MoO_3.

To further prove the presence of O vacancies in MoO_x, the chemical composition of the MoO_x and MoO_3 was probed using X-ray photoelectron spectroscopy (XPS), as shown in Fig. 2. From Fig. 2(a) it can be seen that the major species Mo^{6+} was present in MoO_3. The Mo 3d peak was deconvoluted to obtain the contributions of Mo^{5+} (232.0 eV for Mo 3d5/2) and Mo^{6+} (232.7, 236.0 eV) and the major species present in MoO_x is the mixture of Mo^{5+} and Mo^{6+}, as shown in Fig. 2(b). In addition, Mo^{5+} species was found to be 18.7 atomic rations (%). Mo^{5+} species is the origin of the metal-like

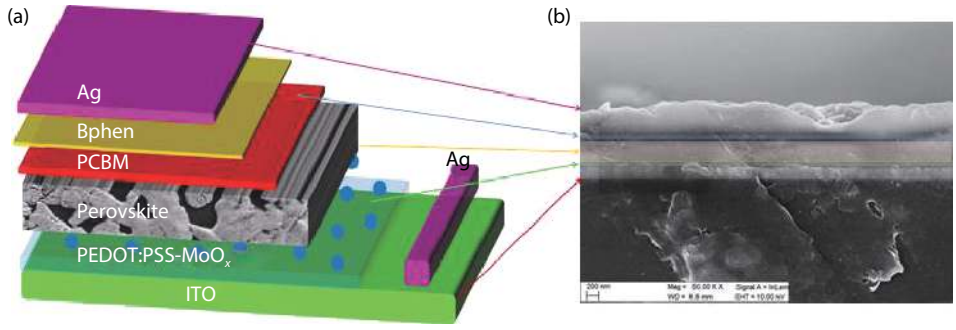

Fig. 3. (Color online) (a) Device construction of the planar PSCs, and (b) cross-sectional SEM image of the planar PSC structures without an Ag electrode.

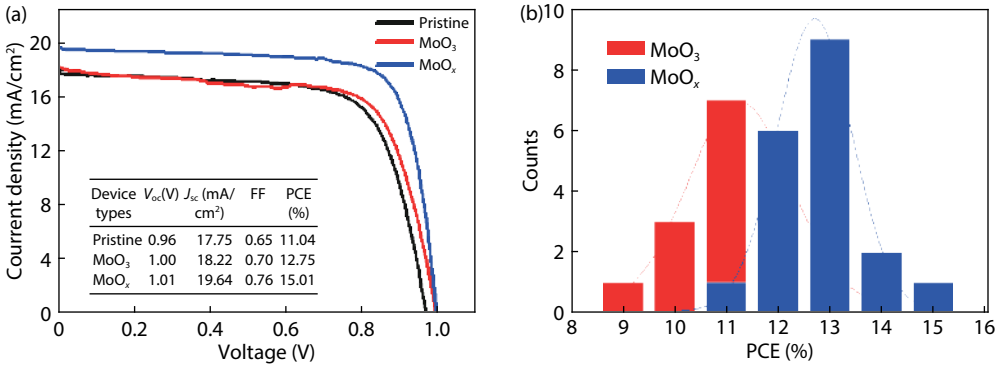

Fig. 4. (Color online) (a) The best *J*–*V* characteristics under illumination for the devices using pristine PEDOT:PSS, PEDOT:PSS-MoO$_x$, and PEDOT:PSS-MoO$_3$ as HTLs. (b) Histogram of PSCs using PEDOT:PSS-MoO$_x$ and PEDOT:PSS-MoO$_3$ as HTLs.

electrical properties of MoO$_x$, which could low the series resistance of solar cell, and be beneficial to collect photo-generated charge carriers and finally enhance J_{sc} of solar cells.

2.3. Device fabrication

The conventional planar architecture is adopted to further prove the effect of MoO$_x$ on the performance of hybrid PSCs, which is constructed with indium tin oxide (ITO)/HTL/$CH_3NH_3PbI_{3-x}Cl_x$/$PC_{61}BM$/Bphen/Ag (Fig. 3(a)). The PEDOT:PSS-MoO$_x$, PEDOT:PSS-MoO$_3$, and PEDOT:PSS were used to fabricate the HTLs. The performance of the devices with these three different HTLs is investigated under AM 1.5 G 100 mW/cm^2 illumination. According to our previous work[27], 1 mol/L concentration of MoO$_x$ and MoO$_3$ is doped into PEDOT:PSS as the holes transport layer. Fig. 3(b) shows the cross-sectional scanning electron microscopy (SEM) image. It can be seen that the perovskite layer completely covered the surface of the HTL layer and had an average thickness of 280 nm.

3. Results and discussion

The current density–voltage (*J*–*V*) characteristics of PSCs using the different HTLs are shown in Fig. 4(a). The relevant performance parameters are also summed up in the inset of Fig. 4(a). Figure 4(b) shows the histogram of PSCs using PEDOT:PSS-MoO$_x$ and PEDOT:PSPS-MoO$_3$. The device with HTL of PEDOT:PSS exhibited a PCE of 11.04%, with V_{oc} of 0.96 V, J_{sc} of 17.75 mA/cm^2, and FF of 0.65. The device with HTL of PEDOT:PSS-MoO$_3$ shows a significantly enhanced PCE of 12.75% with a V_{oc} of 1.01 V, J_{sc} of 18.22 mA/cm^2, and FF of 0.70. Compared to that of the PEDOT:PSS-MoO$_3$ device, the PCE of the PEDOT:PSS-MoO$_x$ device furthermore improved from 12.75 to 15.01%.

By analyzing the data shown in the inset of Fig. 5, we can also see that the FF and J_{sc} values are improved and the series resistances (R_s) are reduced. The values of R_s of the PEDOT:PSS-based cells, PEDOT:PSS-MoO$_3$, and PEDOT:PSS-MoO$_x$ are 18.65, 16.89, and 3.89 Ω·cm^2, respectively. The use of MoO$_3$ NPs additive induces oxidation doping of PEDOT:PSS, which promotes the networking between the conducting PEDOT units, and thereby greatly increases the electric conductivity of hybrid PEDOT:PSS-MoO$_3$ and PEDOT:PSS-MoO$_x$ layer[31].

It is supposed that the significant reduction of R_s ascribes to the good conductivity of PEDOT:PSS-MoO$_x$, and the high hole-conductivity could result in the high J_{sc} and the high FF due to the reduced R_s, which corresponds to the previous report by Nguyen *et al.*[32]. Therefore, the cell photovoltaic performance is strongly affected by the conductivity of the HTLs.

The obvious increase of J_{sc} could be attributed to the incorporation of MoO$_x$ into HTLs and the reduced R_s. Pristine PEDOT:PSS is a poor conductor, resulting in the low charge collection efficiency due to charge reorganization which dominates the charge transfer[33], and causes the devices to suffer from the high R_s. By increasing the conductivity of the HTL with the addition of Mo^{5+}, the ability of the hole transport is improved and the R_s is reduced, which allows improving the charge collection efficiency and increasing J_{sc}. Similar trends of J_{sc} improvements have been observed by using doped spiro-OMeTAD as HTLs[32, 34].

The addition of Mo^{5+} caused the conductivity of the HTL to increase, which resulted in a decrease of R_s, and the reduced R_s greatly affected FF, thus getting an increase in FF[34]. The improved results may be due to the reduced recom-

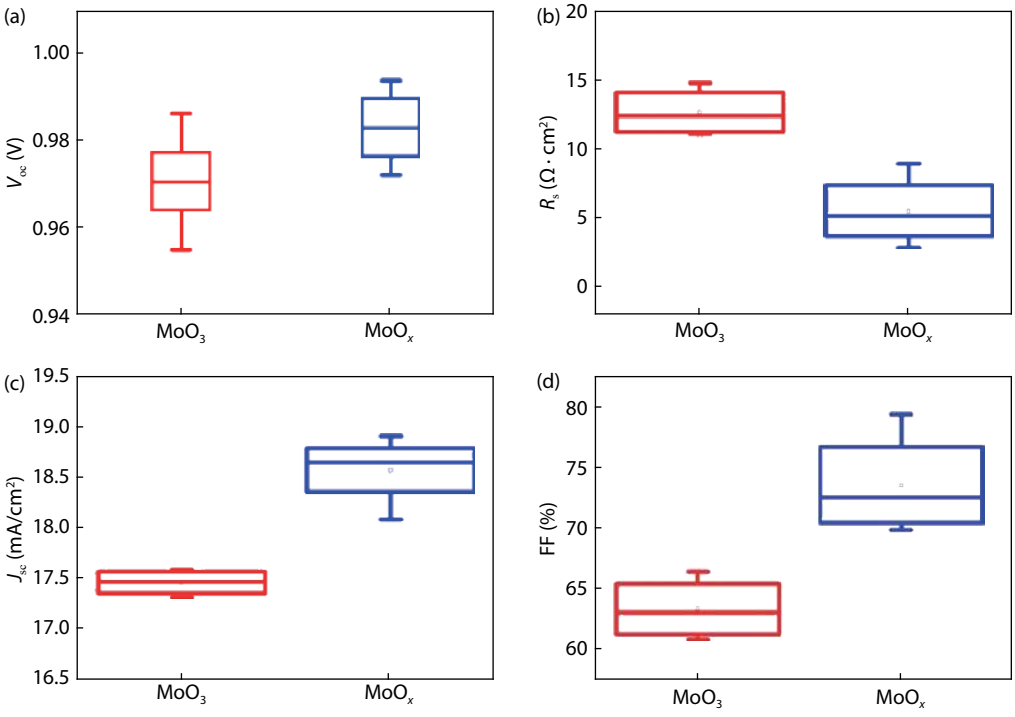

Fig. 5. (Color online) Average photovoltaic parameter for 12 devices: (a) open-circuit voltage (V_{oc}), (b) series resistance (R_s), (c) short-circuit current density (J_{sc}), (d) fill factor (FF).

bination and optimization of the charge transport process caused by the increased conductivity of the HTL layer, which are consistent with previous reports[22, 35].

To further verify what caused the improvements on FF and J_{sc}, the atomic force microscopy (AFM) images and SEM images were carried out to research the surface properties of the HTLs and the perovskite layers. Fig. S1 displays AFM images of the PEDOT:PSS-MoO_3 and PEDOT:PSS-MoO_x, as well as SEM images of perovskite layers on the PEDOT:PSS-MoO_3 and PEDOT:PSS-MoO_x. The PEDOT:PSS-MoO_3 and PEDOT:PSS-MoO_x interface modification had a little effect on the morphology of perovskite films but it is not so obvious. The identical XRD patterns observed from the perovskite films indicated that perovskite crystallizations on PEDOT:PSS-MoO_3 and PEDOT:PSS-MoO_x were the same (Fig. S2). Thus, the difference of photovoltaic performance was solely caused by the different Mo valence states.

To understand the effect of Mo^{5+} on the resistance of the device, Impedance Spectroscopy (IS) measurements were carried out under dark conditions, which provided insights on the charge transport, recombination, and accumulation within the perovskite-based devices[36, 37]. By doing so, the interface characteristics of PSCs can be further clarified by IS. Nyquist plots of the three types of devices measured in dark are shown in Fig. 6. The solid curves are the fitting results with a transmission line model. The measured frequency ranges from 10 to 10^6 Hz with an AC amplitude of 10 mV at 0.8 V bias. These data were used to perform the fitting and to simulate the performance.

The single semicircle appears in Fig. 6, which is consistent with expectation. Moreover, the semi-arc gets smaller as the addition of Mo^{5+} into PEDOT:PSS. We attributed this result to the occupancy of the trap states at the perovskite/HTL interface, which is associated with the presence of a capacitance (C_p)[38]. The equivalent circuit shown in the inset in Fig. 6 could further explain this behavior, where R_s is the series resistance and C_p is the capacitance of the device. These parameters include either contact resistance or the interface of the perovskite/HTL. Since C_p and R_s are strongly depended on the conductivity of the HTLs, the increasing conductivity of the HTLs caused the semi-arcs to become smaller. This signified that the C_p and R_s were decreased significantly, illuminating a lower density of carrier traps at the perovskite/HTL interface. The decreased carrier combination resulted in a smaller C_p[39]. Therefore, the smaller C_p is demonstrated the presence of higher carrier density in the devices with high conductivity of HTLs.

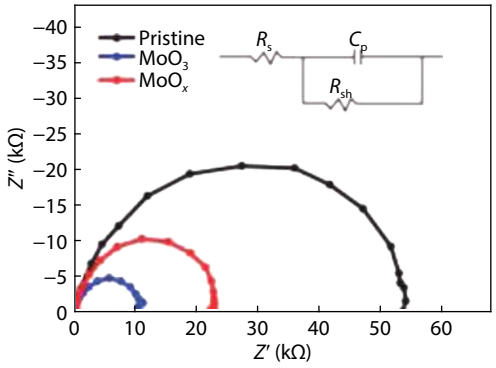

Fig. 6. (Color online) Nyquist plot of devices with various HTLs (pristine PEDOT:PSS, PEDOT:SS-MoO_x and PEDOT:PSS-MoO_3). Solid symbols are experimental results and solid lines are fitted results.

We demonstrated the improved photovoltaic performance by using highly conductive HTLs, namely PEDOT:PSS-MoO_x. Therefore, we will discuss the possible mechanisms for improved performance from the molecular design perspective.

The open-circuit photovoltage decay (OCVD) measure-

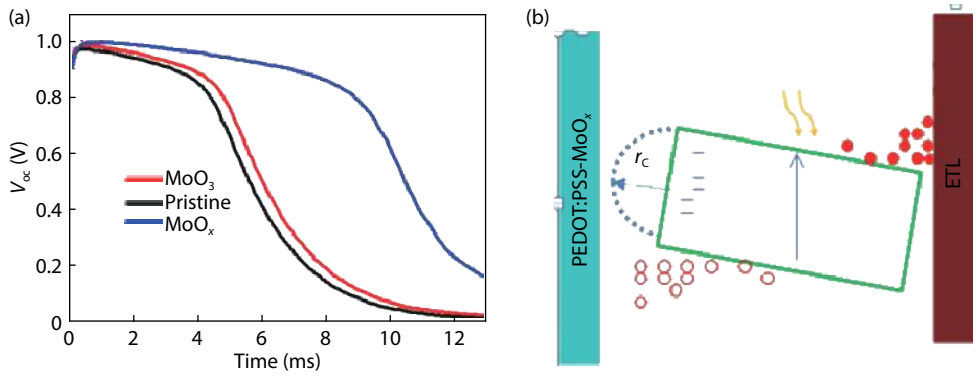

Fig. 7. (Color online) (a) OCVD measurements for three types of devices. (b) Schematic of the proposed mechanism for the trap-assisted recombination.

ments are to establish a photo-stationary state, and the device is illuminated during open circuit[37, 40]. The light is then switched off and the decay in V_{oc} is detected as a function of time. The longer time scales of constant voltage maintaining were detected for the device of PEDOT:PSS-MoO_x HTL as shown in Fig. 7(a). Apparently, a remarkably slow decay of V_{oc} was exhibited for the cell of PEDOT:PSS-MoO_x HTL. The voltage remained at 0.8 V after 9 ms, and it had not completely decayed even at 0.1 s. In contrast, the open-circuit voltage of the cell with pristine PEDOT:PSS or PEDOT:PSS-MoO_3 HTL decayed more speedily, for it only takes 4.5 ms to be below 0.8 V. This observation provided an important insight showing that the highly conductive PEDOT:PSS-MoO_x HTL can maintain a persistent photovoltage at the longer time scales. The slow OCVD decay behavior is similar to the previous report by Baumann *et al.*, in which the TiO_2 ETL was severally replaced by $PC_{70}PCBM$ and MeOTAD HTL was replaced by PEDOT:PSS/polyTPD[41]. Although the origin remains unclear, they speculated that these long-term transients are attributed to the interface presence of the perovskite/TiO_2, which might play an important role in maintaining the slow decaying[37]. They attributed this change of the V_{oc} decay to the onset of a shunt pathway, which decayed the photovoltage more speedily. Our results show a clear change in the photovoltage decays over long periods of time with the highly conductive PEDOT:PSS-MoO_x, and this suggests that the good conductivity of the HTL could reduce the charges recombination which sustains photovoltages decay observed in perovskite solar cells[42].

It is well known that the charge density in the device is closely related to V_{oc} with the following equation:

$$V_{oc} = \frac{kT}{q} \ln \frac{np}{n_0 p_0}, \tag{1}$$

which is supposed that the photovoltage is equal to the quasi Fermi level splitting[43], where k represents the Boltzmann constant, q represents the elementary charge, T represents the temperature, p_0 and n_0 are the intrinsic hole and electron concentrations, and p and n are the total concentrations of electrons and holes, respectively. For the prestine device of PEDOT:PSS under the open circuit conditions, a reduction of concentrations of electrons and holes, which means the increase of the recombination of charges within the device, would result in the decrease of V_{oc}. For the PEDOT:PSS-MoO_x device, the increase of V_{oc} means the reducing recombination of charge carriers, and this result is consistent with the IS measurements results.

The dielectric constants ε_r of the perovskite device based on PEDOT:PSS-MoO_3 and PEDOT:PSS-MoO_x, are tested showed as Fig. 8(a), and the characteristic behavior of the frequency is the real part of the dielectric constant. In low frequency, a significant increase of ε_r of the perovskite device based on PEDOT:PSS-MoO_x is produced compared to that of PEDOT:PSS-MoO_3. At low frequencies—namely, below 10^6 Hz—the dielectric response, ε_r, was assumed to be an ionic conduction, which largely stems from the accumulation of electrode interface charge. In the high-frequency zone, the change of ε_r value is mainly caused by the electronic conduction[44].

The ε_r also affected the recombination of charges in the interface between the perovskite and the HTL. The holes were captured and ended up by the Coulombic interactions between the holes and the negatively charged trap states on the perovskite surface. The trap-assisted reorganization process takes place between the perovskite layer and HTL, as shown by Fig. 7(b). The critical distance (r_c) can be expressed as follows:

$$r_c = \frac{q^2}{4\pi\varepsilon_0\varepsilon_r KT}, \tag{2}$$

where q, ε_0, ε_r, and T are the elementary charge, vacuum permittivity, the dielectric constant of HTL, and temperature, respectively[45]. Under the aid of thermal energy (KT), the charges within the limits of r_c can escape the electrostatic force, and the holes have the greatest probability to be trapped and ended up in HTL within the critical distance[46]. It is obvious that as the ε_r of PEDOT:PSS-MoO_x increases, the r_c value decreases, thus, the probability of trap-assisted recombination within the critical distance of r_c becomes low in the PSCs. This result indicates that the charge accumulation probability at the HTL/perovskite interface is decreased, which is subsequently related to the increase in V_{oc} and J_{sc}. In the device using PEDOT:PSS-MoO_3 as HTL, the r_c value was about 16.8 nm at 295 K, while it was significantly decreased to about 9.1 nm for the PSC based on PEDOT:PSS-MoO_x due to its higher ε_r. Therefore, the electrostatic force can be effectively screened and the trap-assisted recombination could be effectively suppressed in PSCs of PEDOT:PSS-MoO_x. This also explains the reason of the charge recombination effectively

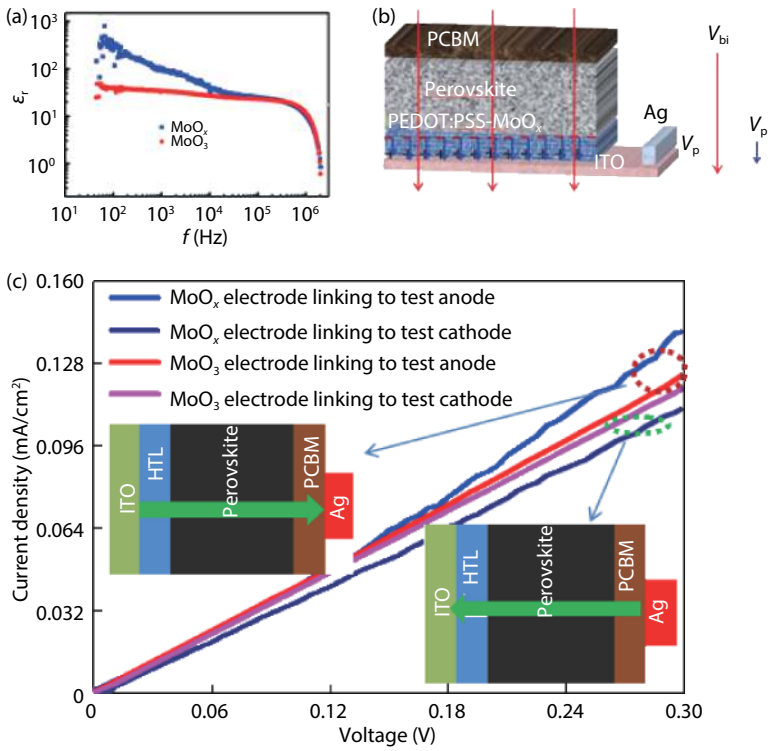

Fig. 8. (Color online) (a) Real part of the dielectric constant as a function of frequency in the dark. (b) Schematic diagram of electric-field distribution in the perovskite device based on PEDOT:PSS-MoO_x. (c) *J*–*V* plots of the perovskite devices based on PEDOT:PSS-MoO_x and PEDOT:PSS-MoO_3 at different scanning directions taken in the dark, inset: the schematic diagraph of testing.

and improved performance of PEDOT:PSS-MoO_x PSCs.

To further distinguish the dielectric constant effect on the polarization performance, the *J*–*V* curves of the same device at the different scanning directions were performed in the dark as shown in Fig. 8(c), which could also explain the possible effect mechanism of interfacial polarization on charge recombination in PSCs. Interfacial polarization was tested with an external bias, as shown in Fig. 8(b). The applied external bias is ranged from 0 to 0.3 V, and *J*–*V* curves were obtained for both devices containing PEDOT:PSS-MoO_x and PEDOT:PSS-MoO_3.

Apart from the impact of MoO_x on conductivity of PEDOT:PSS, the current effect at the different directions of the applied DC field is also studied. The device with a positive electrode linked to a test anode had a similar electron transfer direction to PSC of PEDOT:PSS-MoO_x and PEDOT:PSS-MoO_3. In contrast, a device with a positive electrode linked to a test cathode had an electron transfer direction opposite the two devices. It can be seen from Fig. 8(b) that the measured current and the applied bias are positive correlation. After changing the direction of the applied field, it is found that the current of PSC based on PEDOT:PSS-MoO_3 is very similar to the current before the applied field is changed in the total applied field range. This result suggests that the charge transport in PSC based on PEDOT:PSS-MoO_3 makes no change. Once MoO_3 is changed to MoO_x (with the same electron transfer direction and applied DC power source), the interface induced polarization initiates the electron-hole dipole pairs to separate, then the current is increased. After the direction of the applied field was changed, the current was observed to be measured at room temperature and 0 V applied bias for the perovskite devices based on PEDOT:PSS-MoO_x. The current is lower than that with a positive field in the overall applied field range. This could be clarified to be the significant contribution of interface induced polarization between the perovskite and PEDOT:PSS-MoO_x. When both of the electron transfer directions from the applied DC power source and the interface effect are identical, interface induced polarization initiating the separation of electron-hole dipole pairs could contribute to the increasing current. Fig. 8(c) shows a schematic diagram of electric field distribution in perovskite device based on PEDOT:PSS-MoO_x. The polarization field (E_p) was consistent with the internal built field (E_0). Therefore, it facilitated the separation of photo generated holes and electrons. The accumulated photo-generated holes first at the perovskite/HTL interface are dragged into the PEDOT:PSS-MoO_x layer by E_p and then extracted at the anode, and this reduces the probability of non-radiative recombination by surface and bulk traps in the perovskite layer[47].

4. Conclusion

We have revealed and highlighted the important effect of Mo^{5+} on the conductivity and polarization of HTLs using PSCs. The enhanced conductivity of the HTL by incorporating Mo^{5+} into PEDOT:PSS HTL significantly boosted the photocurrent and reduced charge recombination, which effectively improved device PCES due to the manipulation of the hole pathway by using the more electrically conductive MoO_x and the dielectric constant. We speculated that the higher dielectric constant can produce a polarization field and screen the reorganisation of the traps and the holes in the extraction layer, which could potentially reduce photogenerated charge recombination in the interface of the perovskite and the HTLs. This discovery affords an effective strategy for

structuring efficient charge-transport materials to increase the overall performance of PSCs.

Acknowledgements

This work was supported by Colleges Universities in Henan Province Key Scientific Research Project Funding Scheme (No. 17A140020), Henan Province Nature Science Foundation Project (No. 182300410241) and Chinese Nature Science Foundation Committee (No. 61640406).

References

[1] De Wolf S, Holovsky J, Moon S J, et al. Organometallic halide perovskites: sharp optical absorption edge and its relation to photovoltaic performance. J Phys Chem Lett, 2014, 5(6), 1035

[2] Xing G, Mathews N, Sun S, et al. Long-range balanced electron- and hole-transport lengths in organic-inorganic $CH_3NH_3PbI_3$. Science, 2013, 342(6156), 344

[3] Yoon H, Kang S M, Lee J K, et al. Hysteresis-free low-temperature-processed planar perovskite solar cells with 19.1% efficiency. Energy Environ Sci, 2016, 9(7), 2262

[4] Xing G, Mathews N, Lim S S, et al. Low-temperature solution-processed wavelength-tunable perovskites for lasing. Nat Mater, 2014, 13(5), 476

[5] Heo J H, Im S H, Noh J H, et al. Efficient inorganic–organic hybrid heterojunction solar cells containing perovskite compound and polymeric hole conductors. Nat Photonics, 2013, 7(6), 486

[6] Bryant D, Greenwood P, Troughton J, et al. A transparent conductive adhesive laminate electrode for high-efficiency organic-inorganic lead halide perovskite solar cells. Adv Mater, 2014, 26(44), 7499

[7] Jiang Q, Zhang L, Wang H, et al. Enhanced electron extraction using SnO_2 for high-efficiency planar-structure $HC(NH_2)_2PbI_3$-based perovskite solar cells. Nat Energy, 2016, 2(1), 1

[8] Aeineh N, Barea E M, Behjat A, et al. Inorganic surface engineering to enhance perovskite solar cell efficiency. ACS Appl Mater Interfaces, 2017, 9(15), 13181

[9] Gonzalez-Pedro V, Juarez-Perez E J, Arsyad W S, et al. General working principles of $CH_3NH_3PbX_3$ perovskite solar cells. Nano Lett, 2014, 14(2), 888

[10] Yang K, Fu J, Hu L, et al. Impact of ZnO photoluminescence on organic photovoltaic performance. ACS Appl Mater Interfaces, 2018, 10(46), 39962

[11] NREL chart. http://www.nrel.gov/ncpv/images/efficiency_chart.jpg. 2016

[12] Xie J, Yu X, Sun X, et al. Improved performance and air stability of planar perovskite solar cells via interfacial engineering using a fullerene amine interlayer. Nano Energy, 2016, 28, 330

[13] Kim H, Lim K G, Lee T W. Planar heterojunction organometal halide perovskite solar cells: roles of interfacial layers. Energy Environ Sci, 2016, 9(1), 12

[14] Wang Z K, Gong X, Li M, et al. Induced crystallization of perovskites by a perylene underlayer for high-performance solar cells. ACS Nano, 2016, 10(5), 5479

[15] Liu X, Li B, Zhang N, et al. Multifunctional RbCl dopants for efficient inverted planar perovskite solar cell with ultra-high fill factor, negligible hysteresis and improved stability. Nano Energy, 2018, 53, 567

[16] Hu L, Li M, Yang K, et al. PEDOT:PSS monolayers to enhance the hole extraction and stability of perovskite solar cells. J Mater Chem A, 2018, 6(34), 16583

[17] Qian M, Li M, Shi X B, et al. Planar perovskite solar cells with 15.75% power conversion efficiency by cathode and anode interfacial modification. J Mater Chem A, 2015, 3(25), 13533

[18] Zhao L, Luo D, Wu J, et al. High-performance inverted planar heterojunction perovskite solar cells based on lead acetate precursor with efficiency exceeding 18%. Adv Funct Mater, 2016, 26(20), 3508

[19] Juarez-Perez E J, Wuβler M, Fabregat-Santiago F, et al. Role of the selective contacts in the performance of lead halide perovskite solar cells. J Phys Chem Lett, 2014, 5(4), 680

[20] Bergmann V W, Weber S A, Ramos F J, et al. Real-space observation of unbalanced charge distribution inside a perovskite-sensitized solar cell. Nat Commun, 2014, 5, 5001

[21] Abrusci A, Stranks S D, Docampo P, et al. High-performance perovskite-polymer hybrid solar cells via electronic coupling with fullerene monolayers. Nano Lett, 2013, 13(7), 3124

[22] Tress W, Marinova N, Moehl T, et al. Understanding the rate-dependent *J –V* hysteresis, slow time component, and aging in $CH_3NH_3PbI_3$ perovskite solar cells: the role of a compensated electric field. Energy Environ Sci, 2015, 8(3), 995

[23] Crispin X, Jakobsson F L, Crispin A, et al. The origin of the high conductivity of poly (3, 4-ethylenedioxythiophene)– poly (styrenesulfonate)(PEDOT–PSS) plastic electrodes. Chem Mater, 2006, 18(18), 4354

[24] Zheng X, Bai Y, Xiao S, et al. Strategies for improving efficiency and stability of perovskite solar cells. MRS Adv, 2017, 2, 3051

[25] Huang X, Wang K, Yi C, et al. Efficient perovskite hybrid solar cells by highly electrical conductive PEDOT:PSS hole transport layer. Adv Energy Mater, 2016, 6(3), 1501773

[26] Anusca I, Balčiūnas S, Gemeiner P, et al. Dielectric response: answer to many questions in the methylammonium lead halide solar cell absorbers. Adv Energy Mater, 2017, 7, 1700600

[27] Jiang Y, Li C, Liu H, et al. Poly (3, 4-ethylenedioxythiophene): poly (styrenesulfonate)(PEDOT:PSS)–molybdenum oxide composite films as hole conductors for efficient planar perovskite solar cells. J Mater Chem A, 2016, 4(25), 9958

[28] Wang Z, Lou Y, Naka S, et al. Direct comparison of solution- and vacuum-processed small molecular organic light-emitting devices with a mixed single layer. ACS Appl Mater Interfaces, 2011, 3(7), 2496

[29] Schulz P, Tiepelt J O, Christians J A, et al. High-work-function molybdenum oxide hole extraction contacts in hybrid organic–inorganic perovskite solar cells. ACS Appl Mater Interfaces, 2016, 8(46), 31491

[30] Kim H S, Cook J B, Lin H, et al. Oxygen vacancies enhance pseudocapacitive charge storage properties of MoO_{3-x}. Nat Mater, 2017, 16(4), 454

[31] Lee M H, Chen L, Li N, et al. MoO_3-induced oxidation doping of PEDOT: PSS for high performance full-solution-processed inverted quantum-dot light emitting diodes. J Mater Chem C, 2017, 5(40), 10555

[32] Nguyen W H, Bailie C D, Unger E L, et al. Enhancing the hole-conductivity of spiro-OMeTAD without oxygen or lithium salts by using spiro $(TFSI)_2$ in perovskite and dye-sensitized solar cells. J Am Chem Soc, 2014, 136(31), 10996

[33] Wang N, Zhao K, Ding T, et al. Improving interfacial charge recombination in planar heterojunction perovskite photovoltaics with small molecule as electron transport layer. Adv Energy Mater, 2017, 7(18), 1700522

[34] Li Z, Tinkham J, Schulz P, et al. Acid additives enhancing the conductivity of Spiro-OMeTAD toward high-efficiency and hysteresis-less planar perovskite solar cells. Adv Energy Mater, 2017, 7(4), 1601451

[35] Shao Y, Yuan Y, Huang J. Correlation of energy disorder and open-circuit voltage in hybrid perovskite solar cells. Nat Energy, 2016, 1(1), 1

[36] Dualeh A, Moehl T, Tétreault N, et al. Impedance spectroscopic analysis of lead iodide perovskite-sensitized solid-state solar cells. ACS Nano, 2014, 8(1), 362

[37] Pockett A, Eperon G E, Peltola T, et al. Characterization of planar

lead halide perovskite solar cells by impedance spectroscopy, open-circuit photovoltage decay, and intensity-modulated photovoltage/photocurrent spectroscopy. J Phys Chem C, 2015, 119(7), 3456

[38] Humada A M, Hojabri M, Mekhilef S, et al. Solar cell parameters extraction based on single and double-diode models: A review. Renew Sustain Energy Rev, 2016, 56, 494

[39] Tan F, Qu S, Jiang Q, et al. Interpenetrated inorganic hybrids for efficiency enhancement of PbS quantum dot solar cells. Adv Energy Mater, 2014, 4, 1400512

[40] Liu Z, Niu S, Wang N. Light illumination intensity dependence of photovoltaic parameter in polymer solar cells with ammonium heptamolybdate as hole extraction layer. J Colloid Interface Sci, 2018, 509, 171

[41] Baumann A, Tvingstedt K, Heiber M C, et al. Persistent photovoltage in methylammonium lead iodide perovskite solar cells. Appl Mater, 2014, 2(8), 081501

[42] Tan F, Tan H, Saidaminov M I, et al. In situ back-contact passivation improves photovoltage and fill factor in perovskite solar cells. Adv Mater, 2019, 31(14), 1807435

[43] Shao Y, Xiao Z, Bi C, et al. Origin and elimination of photocurrent hysteresis by fullerene passivation in $CH_3NH_3PbI_3$ planar heterojunction solar cells. Nat Commun, 2014, 5, 5784

[44] Hu L, Sun K, Wang M, et al. Inverted planar perovskite solar cells with a high fill factor and negligible hysteresis by the dual effect of NaCl-doped PEDOT: PSS. ACS Appl Mater Interfaces, 2017, 9(50), 43902

[45] Kuik M, Koster L J, Wetzelaer G A, et al. Trap-assisted recombination in disordered organic semiconductors. Phys Rev Lett, 2011, 107(25), 256805

[46] Sapori D, Kepenekian M, Pedesseau L, et al. Quantum confinement and dielectric profiles of colloidal nanoplatelets of halide inorganic and hybrid organic –inorganic perovskites. Nanoscale, 2016, 8(12), 6369

[47] Brenner T M, Egger D A, Kronik L, et al. Hybrid organic–inorganic perovskites: low-cost semiconductors with intriguing charge-transport properties. Nat Rev Mater, 2016, 1(1), 1